Eur. Phys. J. C 22, 655–666 (2002)
Digital Object Identifier (DOI) 10.1007/s100520100846

THE EUROPEAN PHYSICAL JOURNAL C

Colour dipoles and virtual Compton scattering

M. McDermott[1], R. Sandapen[2], G. Shaw[2]

[1] Division of Theoretical Physics, Department of Math. Sciences, University of Liverpool, Liverpool, L69 3BX, UK
[2] Department of Physics and Astronomy, University of Manchester, Manchester, M13 9PL, UK

Received: 22 July 2001 / Revised version: 5 November 2001 /
Published online: 14 December 2001 –

Abstract. An analysis of Deeply Virtual Compton Scattering (DVCS) is made within the colour dipole model. We compare and contrast two models for the dipole cross-section which have been successful in describing structure function data. Both models agree with the available cross section data on DVCS from HERA. We give predictions for various azimuthal angle asymmetries in HERA kinematics and for the DVCS cross section in the THERA region.

1 Introduction

In this paper we explore the predictions of the colour dipole model for high energy deeply virtual Compton scattering (DVCS):

$$\gamma^*(q) + p(P) \to \gamma(q') + p(P'), \tag{1}$$

where the first photon has spacelike virtuality $q^2 = -Q^2 < 0$, but the second photon is real ($q'^2 = 0$), and hence transversely polarized. DVCS is a particular example of a diffractive process

$$\gamma^*(q) + p(P) \to X + p(P'), \tag{2}$$

in which the diffractively-produced system, X, is separated by a rapidity gap from the elastically-scattered proton (at least for high photon-proton centre-of-mass energies, W, i.e. $W^2 = (q+P)^2 \gg Q^2, M_X^2$). The first HERA data on this process is now available [1,2].

The colour dipole model of diffraction [3] provides a simple unified picture of such diffractive processes and enables "hard" and "soft" physics to be incorporated in a single dynamical framework. At high energies, in the proton's rest frame, the virtual photon fluctuates into a hadronic system (the simplest of which is a $q\bar{q}$ *dipole*) a long distance upstream of the target proton. The formation time of this hadronic system, and of the subsequent formation of the hadronic final state, is much longer than the interaction time with the target. It is this observation that leads to the main (plausible) assumption of the colour dipole model, i.e. that the interaction of a given fluctuation with the target is independent of how it is formed, and is therefore universal. It leads to the following generic factorization of the amplitudes of high energy diffractive processes:

$$\mathcal{A}(\gamma + p \to Xp) = \int \psi_\gamma^{\text{in}} \; \hat{\sigma} \; \psi_X^{\text{out}} \tag{3}$$

where $\hat{\sigma}$ is the interaction cross section of a given configuration with the target and the integral runs over the phase space describing the incoming and outgoing hadronic systems. For the case of dipole scattering, one must integrate over dipole configurations (longitudinal momentum fractions and transverse sizes). We know of no formal proof of this type of high-energy factorization, whether applied to dipoles or more complicated configurations. Nevertheless, within this common framework there are many different formulations for the interaction cross section $\hat{\sigma}$ [4]–[11], which have been applied with varying degrees of success[1]. Here we consider two particular dipole models [6,9] which have both been successful in describing structure function data, but which at first sight differ quite drastically in their structure and implications; and compare their predictions for DVCS.

An additional assumption of most dipole models of diffraction is that the scattering with the target is diagonal with respect to the appropriate variables (i.e. transverse sizes, momentum fractions and polarizations are unchanged by the interaction). For the case of DVCS this implies that the incoming photon must be transversely polarized in order to respect s-channel helicity conservation.

DVCS is a good probe of the transition between soft and hard regimes in the dipole model for two reasons. Firstly, the transverse photon wave function can select large dipoles, even for large Q^2, and certainly for the Q^2 range $2 < Q^2 < 20$ GeV^2 for which data is now available [2]. Secondly, because the final photon is real, DVCS is more sensitive to large dipoles than DIS at the same Q^2, as we shall illustrate quantitatively in Sect. 3. In addition, for $Q^2 \to 0$, the process reduces to real Compton scattering and the cross-section can be reliably inferred from real photo-absorption data, where soft physics dominates.

[1] For a recent overview, see [12]

We stress the potential importance of well-founded dipole descriptions in providing reliable starting points for exploiting DGLAP evolution properties at "large" Q^2. From the theoretical point of view, DVCS is the best understood of all exclusive diffractive processes, essentially because the X system is just a real photon. Indeed, a perturbative QCD factorisation theorem has been explicitly proven as $Q^2 \to \infty$ [13] which enables the QCD amplitude to be described by a convolution in momentum fraction of generalised (or skewed) parton distributions [14] (GPDs) with hard coefficient functions. GPDs correspond to Fourier transforms of operator products evaluated between proton states of unequal momenta (cf. (2)). They are therefore generalizations of the familiar parton distributions of deep inelastic scattering, and like them satisfy perturbative evolution equations [15–18] which enable them to be evaluated at all Q^2 in terms of an assumed input at some appropriate $Q^2 = Q_0^2$. In practice, to compare with experimental results at finite Q^2 one must establish a regime in Q^2 in which the higher twist corrections (see e.g. [19,20]) to this leading twist result are numerically unimportant. This is a very difficult task in general but early indications are that the minimum Q^2 values defining this regime are considerably higher than in inclusive cross sections, for which values as low as $Q_0^2 = 1$ GeV^2, or even lower, have been used. Since the contributions from different transverse sizes are manifest in the dipole model one may realistically hope to gain insight into this question by investigating DVCS in the dipole framework. As such a dipole analysis of DVCS provides a complementary description to the formal QCD analysis, applicable at "large" Q^2. Any insight gained regarding the mixture of soft and hard physics within the dipole model framework, can also be employed in those processes for which factorization theorems have not been proven.

Frankfurt, Freund and Strikman [21] have given a leading order QCD analysis of DVCS. The resulting predictions for the DVCS amplitude at $t = 0$ are in agreement with the recent H1 measurements [2] of the total DVCS cross-section, assuming an exponential t-dependence with a reasonable value of the slope parameter. The GPDs are evolved from an input value $Q_0^2 = 2.6$ GeV^2, where the input GPDs are obtained by estimating their ratio to "ordinary" parton distribution functions (PDFs) using a simple aligned jet model[2]. While this provides a reasonable first estimate, it is clearly subject to uncertainties which will become important when more accurate data are available.

Recently NLO QCD analyses of DVCS have been completed [18,23–25] which use as input GPDs Radyushkin's model [26] based on Double Distributions proportional to PDFs (which automatically impose the correct symmetry properties in the so-called "ERBL region"). The colour dipole model offers a means of estimating these distributions at the input scale in the DGLAP region, in a complementary and well-founded framework, which can accurately describe both virtual Compton scattering and other closely related data over a wide range of Q^2. This is possible because at leading-log accuracy in Q^2, the amplitude is approximately equal to the GPD, at a particular point. In this paper we compute predictions for the cross section of (1), and for various azimuthal angle asymmetries for the associated lepton process [27] which are sensitive to both the real and imaginary parts of the DVCS amplitude.

[2] For further discussion of this approximation, see [22] and the original paper [21]

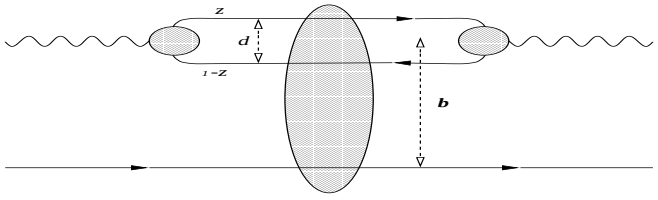

Fig. 1. The colour dipole model for the elastic process $\gamma^* p \to \gamma^* p$(DIS), and virtual Compton scattering $\gamma^* p \to \gamma p$

The structure of the paper is as follows: in Sect. 2 we summarize and compare our two dipole models in the context of deep inelastic scattering; we then discuss their application to virtual Compton scattering process in Sect. 3; compute various observables in Sect. 4 and summarize our results and conclusions in Sect. 5.

2 The colour dipole model

Singly dissociative diffractive γp processes (cf. (2)) are conveniently described in the rest frame of the hadron, in which the incoming photon dissociates into a $q\bar{q}$ pair a long distance, typically of order of the "coherence length" $1/Mx$, from the target proton. Assuming that the resulting partonic/hadronic state evolves slowly compared to the timescale of interaction with the proton or nuclear target, it can be regarded as frozen during the interaction. In the colour dipole model, the dominant states are assumed to be $q\bar{q}$ states of given transverse size, d_T. Specifically

$$|\gamma_r\rangle = \int \mathrm{d}z\ \mathrm{d}^2 d_T\ \psi_r^\gamma(z, d_T, Q^2)\, |z, d_T, \rangle + \dots\ , \qquad (4)$$

where z is the fraction of light cone energy carried by the quark and $\psi_r^\gamma(z, d_T, Q^2)$ is the *light cone wave function* of the photon of polarization $r = T, L$. Assuming that these dominant states are scattering eigenstates (i.e. that z, d_T and the quark helicities, which are left implicit in the above equation, remain unchanged in diffractive scattering) the elastic scattering amplitude for $\gamma^* p \to \gamma^* p$ is specified by Fig. 1. This leads via the optical theorem to

$$\sigma_{T,L}^{\gamma^* p} = \int \mathrm{d}z \mathrm{d}^2 d_T\ |\psi_{T,L}^\gamma(z, d_T, Q^2)|^2 \hat{\sigma}(s^*, d_T, z)\ , \quad (5)$$

for the $\gamma^* p$ total cross-section in deep inelastic scattering, where $\hat{\sigma}(s^*, d_T, z)$ is the total cross-section for scattering dipoles of specified (z, d_T) which do not change in the interaction (the second line then follows from orthogonality and the variable s^* will be specified shortly).

The dipole cross-section is usually assumed to be flavour independent and "geometric", i.e. independent of z. Beyond this the models fall into two main classes.

In the first, the dipole cross-section is assumed to depend solely on the properties of the dipole-proton system itself, implying the choice $s^* = W^2$. Other singly diffractive photo-processes involve exactly the same dipole cross-section, but different wavefunction factors depending on the final state, as we shall see below for virtual Compton scattering.

The second type is more closely connected with hard perturbative QCD predictions for the interaction cross section, which for small x and high Q^2 involve two gluons being exchanged. For hard scattering, small dipoles are connected via two parton lines to the proton. The interaction cross section then depends on the momentum fractions of the proton carried by the parton lines, i.e. $s^* = x_{Bj} = Q^2/W^2$, or $s^* = x' \approx x_{Bj}$. In this case the dipole cross-section must be slightly modified when applying it to different processes, since GPDs of the appropriate kinematics must be used, as discussed below.

In the rest of this section, we shall briefly summarize the properties of one model of each type, after first considering the other main ingredient in (5), i.e. the photon wavefunction.

2.1 The photon wavefunction

Because the proton structure function, F_2, is predominantly transverse, both small and large dipoles contribute significantly to F_2 over a wide range of Q^2, where "large" means transverse sizes of order $d_T \approx 1$ fm. With this caveat, it is none the less useful to consider two qualitatively different regimes.

For small dipoles, it is reasonable to assume "QED wavefunctions," $\psi^{\gamma}_{T,L} = \psi^0_{T,L}$ calculated[3] from the usual QED vertex $-ie\gamma^{\mu}$. Explicitly

$$|\psi^0_L(z, d_T, Q^2)|^2 = \frac{6}{\pi^2}\alpha_{e.m.} \times \sum_{q=1}^{n_f} e_q^2 Q^2 z^2 (1-z)^2 K_0^2(\epsilon d_T) \quad (6)$$

$$|\psi^0_T(z, d_T, Q^2)|^2 = \frac{3}{2\pi^2}\alpha_{e.m.} \times \sum_{q=1}^{n_f} e_q^2 \Big\{ [z^2 + (1-z)^2]\epsilon^2 K_1^2(\epsilon d_T) + m_q^2 K_0^2(\epsilon d_T) \Big\} \quad (7)$$

where

$$\epsilon^2 = z(1-z)Q^2 + m_q^2 \, ,$$

K_0 and K_1 are modified Bessel functions and the sum is over quark flavours. Furthermore, for the large Q^2 values where small dipoles dominate, these wavefunctions become insensitive to the quark mass. In this regime, the wavefunctions are essentially known.

For small $Q^2 \leq 4m_q^2$, the QED wavefunctions become sensitive to the squared quark mass m_q^2. At the same time, large dipoles, for which one would expect significant confinement corrections, become very important. The wavefunction is clearly model dependent in this region.

[3] For an explicit derivation, see Appendix A of [28]

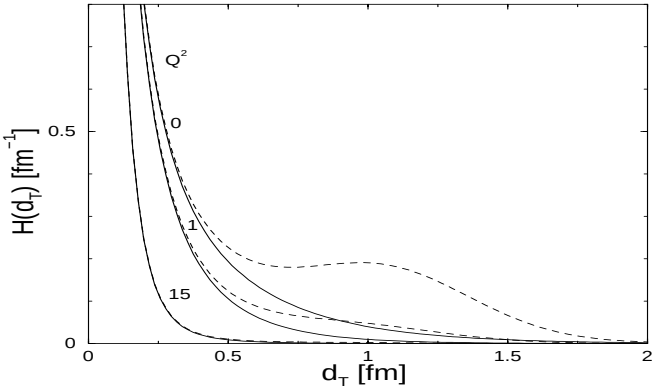

Fig. 2. The weight function $H(d_T)$ for different Q^2 corresponding to the photon wavefunction obtained by FKS [6] with $m_q^2 = 0.08$ GeV^2. The peak at low Q^2 represents the modification to the perturbative photon wave function, with (*dashed line*) and without (*solid line*) the enhancement factor (9) at large d_T

Both of the models discussed in this paper assume that the dipole cross-section becomes "hadron-like" for $d_T \approx 1$ fm, with an energy dependence characteristic of the "soft Pomeron". In choosing the wavefunction in this region, FKS [6] were motivated by the work of Frankfurt, Guzey and Strikman [29]. These authors analyzed the distribution of scattering eigenstates in a non-diagonal generalized vector dominance model [30] which provides a good description of the soft Pomeron contribution to the nucleon structure function F_2 on both protons and nuclei [31]. They found a distribution of states which was qualitatively similar to that obtained in a colour dipole model with a perturbative wavefunction, but with an enhanced contribution from dipole cross-sections of hadronic size. In the light of this, FKS chose $m_q^2 = 0.08$ GeV^2 corresponding roughly to a constituent mass for the light quark case; and modified the QED wavefunction by multiplying by an adjustable Gaussian enhancement factor:

$$|\psi_{T,L}(z, d_T, Q^2)|^2 = |\psi^0_{T,L}(z, d_T, Q^2)|^2 \, f(d_T) \quad (8)$$

where

$$f(d_T) = \frac{1 + B\exp(-c^2(d_T - R)^2)}{1 + B\exp(-c^2 R^2)}. \quad (9)$$

This form enables the width and height of the enhancement to be controlled independently while keeping a factor of close to unity at small d_T. The effect of this is conveniently summarized by integrating out the angular and z dependence in (5) to give

$$\sigma^{\gamma^* p}_{tot} = \int \mathrm{d}z \; \mathrm{d}^2 d_T \; (|\psi_T(z, d_T)|^2 + |\psi_L(z, d_T)|^2)\hat{\sigma}(s, d_T) = \frac{12}{\pi}\alpha_{e.m.} \int \mathrm{d}d_T H(d_T)\hat{\sigma}(s, d_T) \, . \quad (10)$$

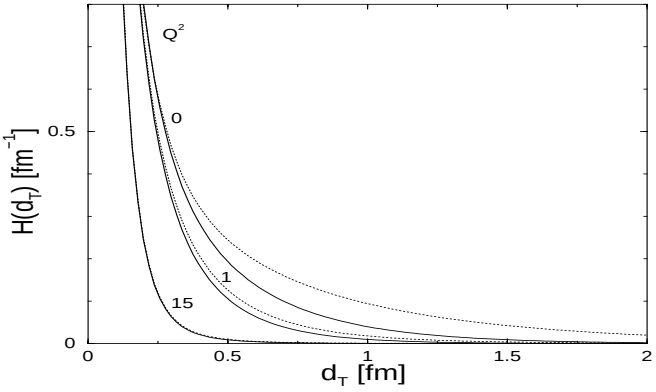

Fig. 3. The weight function $H(d_T)$ for various Q^2 corresponding to photon wavefunctions of perturbative form for $m_q^2 = 0.08$ GeV^2 (solid lines) and $m_q^2 = 0.02$ GeV^2 (dotted lines)

Table 1. Parameters for the FKS model specified by (8, 11), in appropriate GeV based units throughout

λ_S	0.06 ± 0.01	λ_H	0.44 ± 0.01
a_0^S	30.0(fixed)	a_2^H	0.072 ± 0.010
a_4^S	0.027 ± 0.007	a_6^H	1.89 ± 0.03
		ν_H	3.27 ± 0.01
B	7.05 ± 0.08	c^2	0.20(fixed)
R	6.84 ± 0.02		
m_q^2	0.08(fixed)	m_c^2	1.4(fixed)

The resulting behaviour of $H(d_T)$ for the final parameter values (see below) is shown in Fig. 2: as can be seen, the enhancement is important for very low Q^2, but decreases rapidly as Q^2 increases. Other authors do not in general include an explicit enhancement factor, but achieve a similar effect, at least for $Q^2 > 1$ GeV^2, by varying the quark mass. Choosing a smaller quark mass increases the wavefunction at all large d_T, as illustrated in Fig. 3. Golec-Biernat and Wusthoff [5], for example, used $m_q^2 = 0.02$ GeV^2, comparable with the pion mass squared.

For our second model, the MFGS model [9], this question is less important, since results are only presented for $Q^2 > 1$ GeV^2; and results are presented for $m_q^2 = 0.08$ GeV^2 without the confinement factor of (9). In both models, a charmed quark contribution has also been included, which only differs from the up quark contribution by the quark mass $m_c = 1.4$ GeV.

Given this uncertainty in the wavefunction, it is clear from (5) that the dipole cross-section at large $d_T \approx 1$ fm cannot be inferred, even in principle, from structure function and real photo-absorption data alone. Other information must also be used.

2.2 The FKS model

This model [6] belongs to the class in which the dipole cross-section is assumed to depend solely on the properties of the dipole-proton system itself, implying the choice $s^* = W^2$ independent of the virtuality of the incoming (or outgoing) photon. The idea was then to extract information on the dipole cross-section by assuming a reasonable but flexible parametric form to fit structure function and real photoabsorption data in the diffractive region $x \leq 0.01$ for $0 \leq Q^2 < 60$ GeV^2. This was implemented by assuming a sum of two terms

$$\hat{\sigma}(W^2, d_T) = \hat{\sigma}_{\rm soft}(W^2, d_T) + \hat{\sigma}_{\rm hard}(W^2, d_T)\,, \qquad (11)$$

each with a Regge type energy dependence on the dimensionless energy variable $d_T^2 W^2$:

$$\hat{\sigma}_{\rm soft}(W^2, d_T) = a_0^S \left(1 - \frac{1}{1 + a_4^S d_T^4}\right) (d_T^2 W^2)^{\lambda_S} \qquad (12)$$

$$\hat{\sigma}_{\rm hard}(W^2, d_T) = (a_2^H d_T^2 + a_6^H d_T^6) \times \exp(-\nu_H d_T)(d_T^2 W^2)^{\lambda_H}\,. \qquad (13)$$

These functions were chosen[4] so that for small dipoles the hard term dominates yielding a behaviour

$$\hat{\sigma} \to a_2^H d_T^2\ (d_T^2 W^2)^{\lambda_H} \qquad d_T \to 0$$

in accordance with colour transparency ideas. For large dipoles the soft term dominates with a hadron-like behaviour

$$\hat{\sigma} \approx a_0^S\ (d_T^2 W^2)^{\lambda_S} \qquad d_T \approx 1 \text{ fm}.$$

The values $\lambda_S \approx 0.06$, $\lambda_H \approx 0.44$ resulting from the fit are characteristic of the soft and hard Pomeron respectively, but the fits could be obtained for a range of values for the parameter a_0^S because of the uncertainty in the photon wavefunction at large d_T discussed above. This ambiguity can be resolved by using the same dipole cross-section to calculate the structure function, $F_2^{D(3)}(x, Q^2, M_X^2)$, for diffractive deep inelastic scattering (DDIS)

$$\gamma^* + p \to X + p \qquad (14)$$

and a subsequent paper [7] showed that good agreement was found for $a_0^S \approx 30$ GeV^{-2}. The parameter values for this fit are given in Table 1 and the resulting behaviour of the dipole cross-section as a function of d_T is shown in Fig. 4 for three energies, including $W = 75$ GeV corresponding to the mean energy of the virtual Compton scattering data [2] to be discussed below.

One feature of the FKS model is that, in its present form, it does not include "gluon saturation" or "unitarity corrections" which are expected to eventually damp the rapid rise with energy of the dipole cross-section for small dipoles. Its success implies that such effects are not necessarily required in the HERA region. However, by examining the predicted behaviour of the dipole cross-section,

[4] In [6] a more complicated parametric form was used, but this simpler parametric form gives very similar results

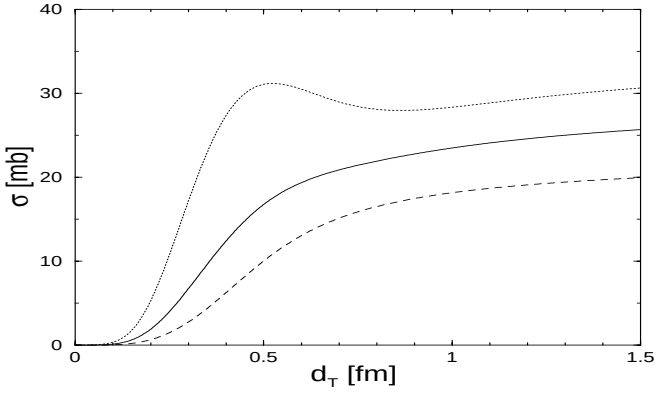

Fig. 4. The FKS dipole cross section at $W = 10, 75, 300$ GeV (dashed, solid and dotted lines, respectively)

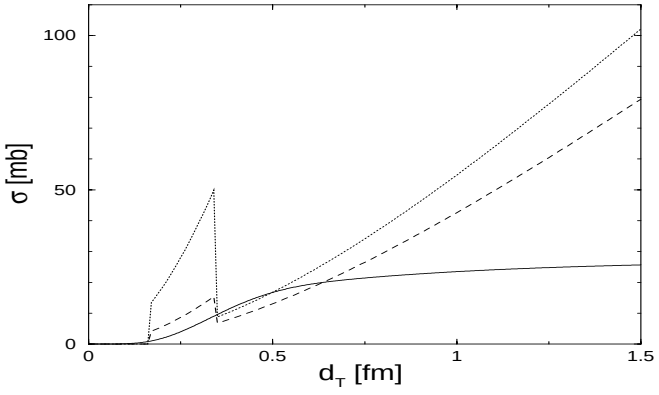

Fig. 5. The Donnachie-Dosch dipole cross section [11] at $W = 75$ GeV (dashed line) and $W = 300$ GeV (dotted line). The FKS dipole cross-section at $W = 75$ GeV (solid line) is included for comparison

the authors have argued [8] that saturation effects will begin to play a role at the top of the HERA range and will rapidly become important above it. This is illustrated in Fig. 4, which shows that the rapidly rising dipole cross-section at small d_T, where the hard term dominates, reaches hadronic sizes at the top of the HERA range $W \approx 300$ GeV.

Finally, for completeness, in Fig. 5 we compare the FKS dipole cross-section with that used in a recent analysis of DVCS by Donnachie and Dosch [11]. This model associates dipoles whose sizes are less than (or greater than) a certain critical size with a fixed power energy dependence corresponding to the hard (or soft) Pomeron respectively[5]. For dipoles whose transverse size is less than about 0.8 fm, the resulting behaviour is not unlike the FKS dipole cross-section at $W = 75$ GeV, which is the mean energy of the data, and the model gives a good account of H1 data in this region. However at higher energies the model develops a rather artificial dependence on the dipole size: as can be seen from the dotted curve in Fig. 5 for $W = 300$ GeV, the dipole cross section not only does not increase monotonically with dipole size, but develops a large discontinuity at the matching point ($d_\perp \approx 0.3$ fm). The other obvious difference is that the cross-section is much larger than the FKS cross-section at large d_T. However for DIS this can be compensated by differences in the photon wave-function, which is uncertain in this region, as noted at the end of Sect. 2.1. FKS resolved this ambiguity by considering the DDIS reaction of (14), which is more sensitive to large dipoles and involves a strikingly different combination of wavefunction and cross-section. It would be interesting to see the predictions of the Donnachie-Dosch model for this reaction.

2.3 The MFGS model

This model [9,10] is directly based on the known behaviour of hard small-x QCD processes, i.e. that they are driven by the gluon distribution at small x. Using the phenomena of colour transparency, it directly relates the dipole cross-section at small d_T to leading order (LO) gluon distributions at large Q^2. To leading order in $\ln Q^2$, and within the small x limit, the total photon-proton cross-sections are given by expressions of the form (5) with a QED wave-function and a dipole cross-section[6]

$$\hat{\sigma}_{\rm pQCD}(x, d_T) = \frac{\pi^2 d_T^2}{3} \alpha_s(\bar{Q}^2) x g(x', \bar{Q}^2)\,, \qquad (15)$$

where $xg(x', \bar{Q}^2)$ is the LO gluon distribution of the proton. At leading log it is sufficient to choose $x' = x$ and $\bar{Q}^2 = Q^2$. However in the MFGS model (specified fully in [9]) an attempt to go beyond leading log was made by introducing d_T-dependence into the scales, x' and $\bar{Q}^2$. For the four momentum scale $\bar{Q}^2$, the phenomenological relation

$$\bar{Q}^2 = \frac{\lambda}{d_T^2} \qquad (16)$$

was assumed where $\lambda = \langle d_T^2 \rangle Q^2$. A theoretical procedure for defining $\langle d_T^2 \rangle$ using the integral in d_T for F_L in [33] gave a value of $\lambda \approx 10$. This value was used in [9], but it was later discovered that the inclusive cross sections are rather insensitive to its precise value in the range $\lambda = 4 - 15$ and that the lower value of $\lambda = 4$ appears to be favoured by the J/ψ-photoproduction data [10]. We adopt this lower value in what follows. The momentum fraction required to create a quark-antiquark pair of mass $M_{q\bar{q}}^2 = (k_T^2 + m_q^2)/(z(1-z))$ is

$$x' = \frac{M_{q\bar{q}}^2 + Q^2}{Q^2 + W^2}\,; \qquad (17)$$

since k_T is Fourier conjugate to d_T the following relationship was adopted [9] for a dipole of given transverse size d_T:

$$x' = x \left[1 + 0.75 \frac{\lambda}{d_T^2 (Q^2 + 4 m_q^2)} \right]\,. \qquad (18)$$

[5] In contrast the FKS model has both hard and soft components for all sizes, but in smoothly varying amounts

[6] This formula is implicit in most perturbative two gluon models. For an explicit derivation see [32]

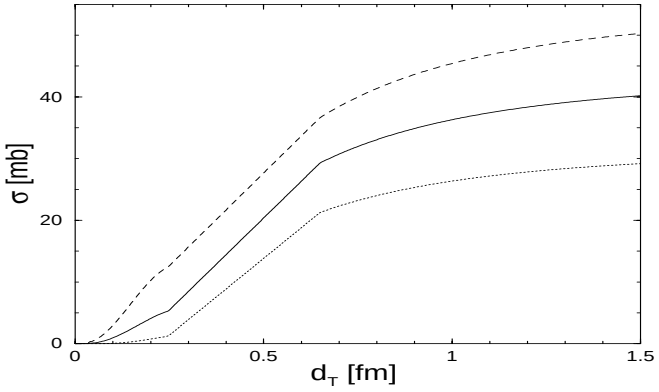

Fig. 6. The MFGS dipole at $W = 10, 75, 300$ GeV (dotted, solid and dashed lines, respectively) at fixed $Q^2 = 1$ GeV^2, corresponding to $x \approx 10^{-2}, 2.10^{-4}$ and 10^{-5}, respectively

The dipole cross-section was then evaluated using the CTEQ4L gluon distributions [34] for a region $d_T \leq d_{T,c}$ in which (15) is appropriate, where the boundary $d_{T,c}$ is specified below. For large dipoles $d_T \geq d_{T,\pi} = 0.65$ fm, the form

$$\hat{\sigma}(d_T > d_{T,\pi}) = \hat{\sigma}(\pi P) \frac{3\, d_T^2}{2\, d_T^2 + d_{T,\pi}^2} \left(\frac{x_0}{x}\right)^{0.08}, \qquad (19)$$

with an x-dependence characteristic of soft Pomeron exchange, is used, where $x_0 = 0.01$ and the value at $d_T = d_{T,\pi}$, $x = x_0$ is matched to the pion-proton total cross-section, $\sigma(\pi P) = 24$ mb. In the intermediate region $d_{T,c} < d_T < d_{T,\pi}$, the dipole cross-section was linearly interpolated between the boundary values at $d_{T,c}$ and $d_{T,\pi}$.

For moderate x, the point $d_{T,c}$ is set by the boundary of the perturbative region in d_T: $d_{T,c} = d_{T,0} \equiv \sqrt{\lambda/Q_0^2} = 0.246$ fm, for $Q_0 = 1.6$ GeV which is the starting scale for the CTEQ4L partons (below this scale they are not defined). The resulting dipole cross-section for $Q^2 = 1$ GeV^2 is shown in Fig. 6 for various values of W.

At small enough x, as a result of the rising gluon density, the small dipole cross section increases faster than the large dipole one and soon reaches hadronic size (tens of mb). This threatens to spoil the monotonic increase of $\hat{\sigma}$ with d_T. To prevent this the MFGS model implements taming corrections that guarantee that the small dipole cross section cannot reach more than half its value at $d_{T,\pi}$. This constraint implies a $d_{T,c}$ that shifts to increasingly small d_T. This correction is not crucial in the HERA region for $\lambda = 4$, but does becomes important above it.

The parameters of the model are not adjusted to fit data, but nonetheless good semi-quantitative accounts of the deep inelastic scattering [9] and J/ψ photoproduction data [10] were obtained. For exclusive diffractive processes, such as vector meson production or DVCS, it is necessary to include GPDs, parameterized in terms of skewedness, δ, x' and $\bar{Q}^2$, rather than the ordinary ones used in (15). For DVCS, $\delta = x_{Bj} = Q^2/2P.q$. To implement leading order GPDs, we adapted the skewed evolution package developed by Freund and Guzey [35], using the CTEQ4L gluon distributions [34] as input to the LO skewed evolution.

The model focuses on small dipoles, and while the behaviour for large dipoles is a sensible guess, no detailed attempt to resolve the intrinsic ambiguity in the wavefunction and cross-section for large dipoles discussed earlier has been made. In what follows we shall restrict this model to $Q^2 > 1$ GeV^2, where one is relatively insensitive to this region due to the smallness of the wavefunction.

3 Virtual Compton scattering

In the colour dipole model, virtual Compton scattering is again given by Fig. 1, but with a real photon in the final state, leading to

$$Im\ \mathcal{A}^{\rm DVCS}(W^2, Q^2, t = 0) = \int dz\ \mathrm{d}^2 d_T\ \psi_T^*(z, d_T, Q^2) \hat{\sigma}(s^*, z, d_T)\ \psi_T(z, d_T, 0)\,, \qquad (20)$$

for the imaginary part of the DVCS amplitude at zero momentum transfer. Thus, our dipole models yield no-free-parameter predictions for this process. In this section we compare the predicted behaviours of the amplitude in the two models, leaving the comparison between predictions and experiment to Sect. 5.

We start by comparing the contributions to the amplitude arising from dipoles of different size. To do this we perform the angular and z integrations to rewrite (20) in the form

$$Im\ \mathcal{A}(W^2, Q^2, t = 0) = 2\pi \int \mathrm{d}d_T\ p(d_T, s, Q^2)\,, \qquad (21)$$

where the profile function

$$p(d_T, s^*, Q^2) = \int dz\ d_T\ \psi_T^*(z, d_T, Q^2)\ \hat{\sigma}(s^*, z, d_T) \psi_T(z, d_T, 0)\,, \qquad (22)$$

gives the relative contributions arising from dipoles of different size d_T. The results are shown for both models at the mean energy, $W = 75$ GeV, of the H1 data in Figs. 7, 8. As Q^2 increases, the profile shifts to smaller d_T. The FKS model has a larger contribution from large dipoles than the MFGS model, although the forward amplitudes, obtained by integrating over all transverse sizes, are similar over a wide range of W and Q^2, as we shall see.

It is also interesting to compare (22) to the corresponding profile function

$$\tilde{p}_T(d_T, s^*, Q^2) = \int dz\ d_T\ \psi_T^*(z, d_T, Q^2) \times \hat{\sigma}(s^*, z, d_T)\ \psi_T(z, d_T, Q^2)\,, \qquad (23)$$

for the forward Compton scattering amplitude in which both transverse photons have the same Q^2, which is related by the optical theorem to the transverse cross-section in DIS. The characteristic behaviour differences observed between DIS and DVCS are illustrated in Figs. 9

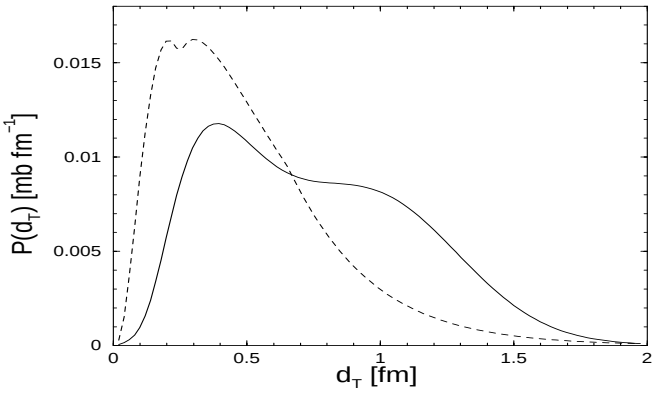

Fig. 7. Profile in transverse dipole size for $Q^2 = 1$ GeV^2 and $W = 75$ GeV, employing the FKS (solid line) and MFGS (dashed line) models for the dipole cross section

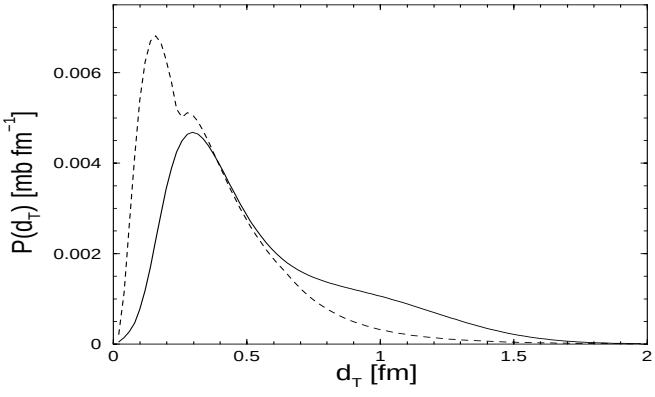

Fig. 8. Profile in transverse dipole size for $Q^2 = 10$ GeV^2 and $W = 75$ GeV, employing the FKS (solid line) and MFGS (dashed line) models for the dipole cross section

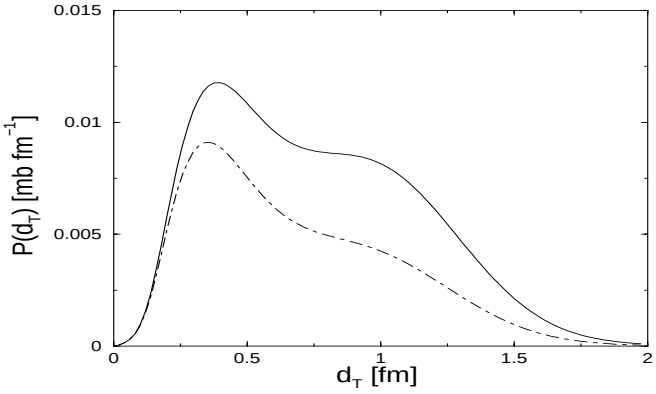

Fig. 9. Comparison of the profile functions of (22, 23) for DVCS (solid line) and transverse DIS (dot-dash line) respectively at $Q^2 = 1$ GeV^2 and $W = 75$ GeV, employing the FKS model for the dipole cross section

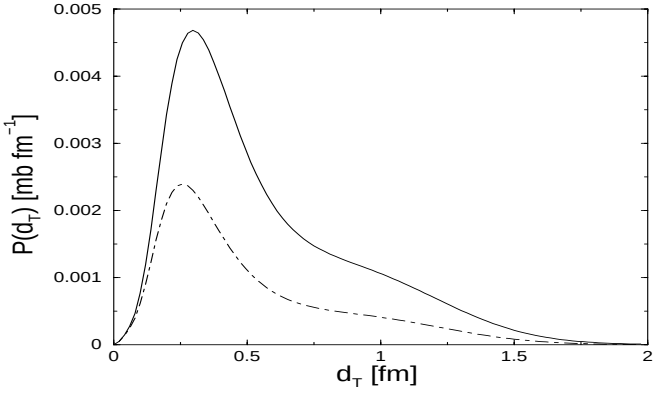

Fig. 10. Comparison of the profile functions of (22, 23) for DVCS (solid line) and for transverse DIS (dot-dash line) at $Q^2 = 10$ GeV^2 and $W = 75$ GeV, employing the FKS model for the dipole cross section

and 10, using the FKS dipole model. For $Q^2 = 0$ the two profiles are obviously identical, and for all Q^2 they become identical for small d_T, since to leading order in $1/d_T$, the transverse wavefunction

$$|\psi_T^0(z, d_T, Q^2)|^2 \to \frac{3}{2\pi^2}\alpha_{e.m.}\sum_{q=1}^{n_f} e_q^2 \frac{z^2 + (1-z)^2}{d_T^2} \quad (24)$$

independent of Q^2. However, as can be seen, when Q^2 increases the large dipoles are less suppressed in the DVCS case than in the DIS case, so that the former is the "softer" process at any given Q^2.

Returning to DVCS, the imaginary part of the amplitude is trivially obtained by integrating (21) over all d_T. In the FKS model we have a sum of two Regge contributions, and the real part is easily computed from the corresponding signature factors; for the MFGS model, results were obtained using dispersion relations, as in [10]. The results for real and imaginary parts, using both models, are plotted as a function of W in Fig. 11 at the mean Q^2 of the H1 data, and the ratio is plotted in Fig. 12. We extend the energy range out to the THERA range (see e.g. [36]) and one can clearly see that the FKS model has a steeper energy dependence at very high energies.

Finally, in our introduction we noted that in [21], the ratio

$$R \equiv \frac{Im\ \mathcal{A}(\gamma^* N \to \gamma^* N)_{t=0}}{Im\ \mathcal{A}(\gamma^* N \to \gamma N)_{t=0}} \quad (25)$$

of the imaginary parts of the forward amplitudes for DIS and DVCS was estimated at the input $Q^2 = 2.6$ GeV^2 using a simple aligned jet model, in order to infer the input generalized parton distributions for QCD evolution. Explicitly, this model gives [21]

$$R = \frac{Q^2}{Q^2 + M_0^2}\ \ln^{-1}(1 + Q^2/M_0^2) \quad (26)$$

where M_0^2 is estimated to be in the range 0.4 - 0.6 GeV^2. The predictions of our models are compared with (26) in Fig. 13, suggesting somewhat larger values at $Q^2 = 2.6$ GeV^2, as can be seen.

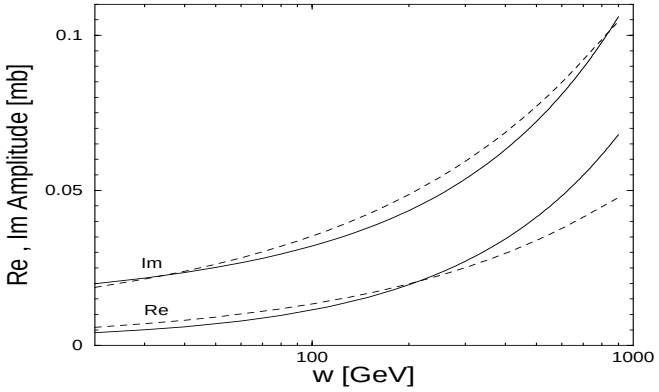

Fig. 11. Real and imaginary parts of the DVCS amplitude for the FKS (solid lines) and MFGS (dashed lines) dipole models for $Q^2 = 4.5$ GeV^2

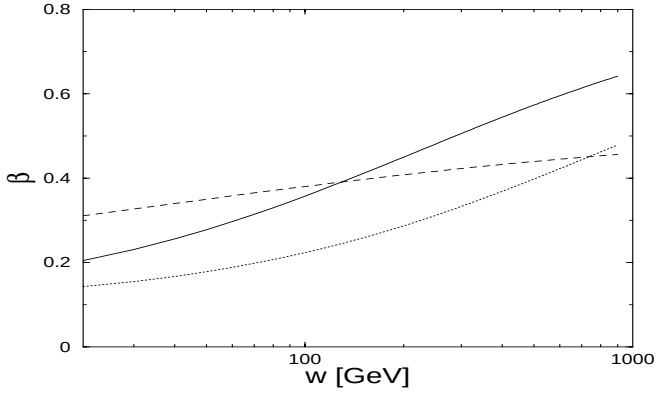

Fig. 12. The ratio, β, of the real to imaginary parts of the DVCS forward amplitude at $Q^2 = 4.5$ GeV^2: FKS (solid line); MFGS (dashed line); and FKS at $Q^2 = 0$ GeV^2 (dotted line)

4 The lepton level process

4.1 Definition of the DVCS cross section

Virtual Compton scattering is accessed experimentally through the leptonic process:

$$e^{\pm}(k) + p(P) \to e^{\pm}(k') + p(P') + \gamma(q') \qquad (27)$$

where the four momenta of the incoming and outgoing particles are given in brackets. As well as DVCS, the Bethe-Heitler process (BH), in which the photon is radiated by the initial or final state lepton, also contributes. On integrating over the azimuthal angle (defined below), the interference term between the two processes vanishes in the limit of large Q^2, and the differential cross-section can be written as:

$$\frac{d^2\sigma}{dydQ^2} = \frac{d^2\sigma^{DVCS}}{dydQ^2} + \frac{d^2\sigma^{BH}}{dydQ^2}\,,$$

where $y \equiv (k - k') \cdot P/(k \cdot P)$ and $Q^2 = -(k - k')^2$. For DVCS, Q^2 is the magnitude of the virtuality of the (spacelike) virtual photon and, in the proton's rest frame, y is the fraction of the incoming electron energy carried by the virtual photon. Neglecting the lepton and proton masses we have $y \approx (Q^2 + W^2)/S$, where $S = (k + p)^2$ is the square of the lepton-proton centre-of-mass energy. The Bethe-Heitler contribution is essentially known in terms of the Dirac and Pauli form factors (see e.g. (18, 27) of [27]) and can be easily calculated and subtracted from the total to leave

$$\frac{d^2\sigma^{DVCS}}{dydQ^2} = \frac{\alpha_{e.m.}}{2\pi Q^2 y}\,\left[1 + (1-y)^2\right]\,\sigma(\gamma^* p \to \gamma p)\,. \qquad (28)$$

Making a trivial change of variable from y to $W = \sqrt{(k - k' + P)^2}$ yields:

$$\frac{d^2\sigma^{DVCS}}{dWdQ^2} = \frac{\alpha_{e.m.}}{\pi Q^2 W}\,\left[1 + (1-y)^2\right]\,\sigma(\gamma^* p \to \gamma p)\,. \qquad (29)$$

We now have a convenient form for comparing to the data on $\sigma(\gamma^* P \to \gamma p)$ which is binned in Q^2 and W. Assuming the usual exponential dependence in $t = (p - p')^2 < 0$, i.e. e^{Bt}, the total $\gamma^* - p$ cross section is given by:

$$\sigma(\gamma^* p \to \gamma p) = \frac{1}{B}\,\left.\frac{d\sigma}{dt}\right|_{t=0}\,, \qquad (30)$$

where, with our definition for $\mathcal{A}^{DVCS}$,

$$\left.\frac{d\sigma}{dt}\right|_{t=0} = \frac{(\mathrm{Im}\mathcal{A})^2}{16\pi}\,(1 + \beta^2) \qquad (31)$$

and β is the ratio of the real to the imaginary part of the forward virtual Compton scattering amplitude $\mathcal{A}$ at $t = 0$.

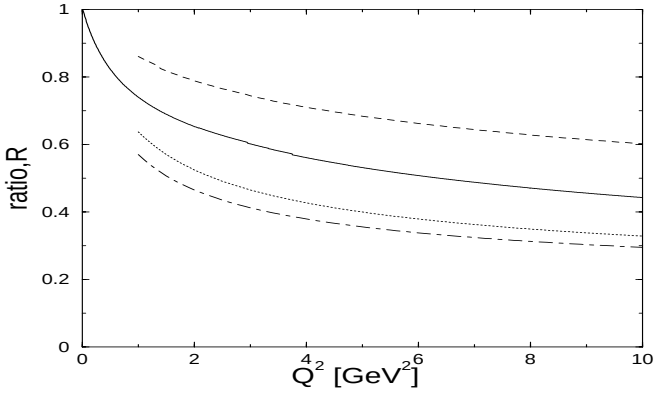

Fig. 13. The ratio of the forward amplitudes for DIS and DVCS (cf. (25)) at $W = 75$ GeV: FKS (solid line); MFGS (dashed line); and the prediction of (26) for $M_0^2 = 0.6$ GeV^2 (dotted line) and $M_0^2 = 0.4$ GeV^2 (dot-dashed line), respectively

4.2 Definitions of asymmetries

A unique and attractive feature of DVCS is the interference with the Bethe-Heitler process which offers the rare chance to isolate both real and imaginary parts of the diffractive amplitude via azimuthal angle asymmetries [27]. These asymmetries are conveniently discussed

in a special frame [19] with the proton at rest such that the direction of the vector $q \equiv k - k'$ defines the negative z-axis. Without loss of generality we can choose the incoming electron to have only a non-zero component along the positive x-axis in the transverse $(x-y)$ plane. In this frame we have the following four-vectors:

$$k = (k_0, k_0 \sin\theta_e, 0, k_0 \cos\theta_e),$$
$$q = (q_0, 0, 0, -|q_3|) \tag{32}$$

$$P = (M, 0, 0, 0), \tag{33}$$
$$P' = (P'_0, |\mathbf{P}'| \cos\phi \sin\theta_H, |\mathbf{P}'| \sin\phi \sin\theta_H, |\mathbf{P}'| \cos\theta_H),$$

where the angle of interest, ϕ, is the azimuthal angle between the lepton $(x-z)$ and hadron scattering planes.

The motivation for using this frame is that the frame-dependent expression for the $u-$channel BH lepton propagator has a particularly simple Fourier expansion in the angle ϕ. In [27] a slightly different frame is used and an explicit expression for the $u-$channel propagator is given, up to terms of order $\mathcal{O}(1/Q^3)$ (cf. (21) of [27]):

$$(k - q')^2 = -\frac{(1-y)Q^2}{y} (A_0 + A_1 \cos\phi + A_2 \cos 2\phi + \cdots), \tag{34}$$

where

$$A_0 = 1 - \frac{t}{Q^2}\left(\frac{1}{2} + \frac{(1-x)(1-2\,t_{\min}/t)}{(1-y)}\right),$$
$$A_1 = 2\sqrt{\frac{-t}{Q^2}}\sqrt{\frac{(1-t_{\min}/t)(1-x)}{(1-y)}}. \tag{35}$$

In the frame used here [19] the Fourier series terminates at $\cos\phi$ ($A_n = 0, n \geq 2$). We explicitly include factors of $1/(A_0 + A_1\cos\phi)$ as appropriate in our numerical results. We use a code written for [24] which approximately implements (18) and (24,27,30) of [27] (the latter neglect terms of $\mathcal{O}(1/Q)$, i.e. they use $A_0 = 1$ and $A_1 = 0$). The code includes the above expansion of the $u-$ channel BH lepton propagator in our frame (taking its full ϕ and y-dependence into account, up to corrections of $\mathcal{O}(1/Q^3)$). The asymmetries of interest involve the quadruple differential cross section on the lepton level

$$d\sigma^{DVCS+BH} = \frac{d\sigma^{(4)}(ep \to ep\gamma)}{dx dQ^2 dt d\phi}.$$

In order to proceed it was necessary to convert our amplitude (cf. (20)) to the dimensionless unpolarized helicity non-flip amplitude, $\mathcal{H}_1$, appearing in (24,27,30) of [27], since at small x and moderate t the contributions of the polarized, $\tilde{\mathcal{H}}_1, \tilde{\mathcal{E}}_1$, and unpolarized helicity-flip, $\mathcal{E}_1$, DVCS amplitudes are negligible. Assuming a simple exponential $t-$dependence on the amplitude level the conversion factor is:

$$\mathcal{H}_1 = \exp(Bt/2)\frac{W^2}{4\pi\alpha_{e.m.}\,\hbar c} A^{\text{dipole}} \tag{36}$$

where W is in units of GeV, so the standard conversion factor $\hbar c = 0.389$ GeV^2 mb is necessary to make $\mathcal{H}_1$ dimensionless.

Using the special frame defined above to specify the azimuthal angle, the asymmetries are defined as follows (see also [24]):

– The (unpolarized) azimuthal angle asymmetry (AAA), measured in the scattering of an unpolarized probe on an unpolarized target, is defined by

$$\text{AAA} = \Big\{\Big(\int_{-\pi/2}^{\pi/2} d\phi (d\sigma^{DVCS+BH} - d\sigma^{BH}) - \int_{\pi/2}^{3\pi/2} d\phi (d\sigma^{DVCS+BH} - d\sigma^{BH})\Big)\Big/ \Big(\int_0^{2\pi} d\phi (d\sigma^{DVCS+BH} - d\sigma^{BH})\Big)\Big\} \tag{37}$$

where $d\sigma^{BH}$ is the pure BH term. The above approximation for the $u-$channel BH propagator leads to a non-trivial $\phi-$dependence of the pure BH term. To directly access the DVCS amplitudes, via the interference term, we define AAA with this piece subtracted. Note that with this "subtracted definition" the magnitude of AAA may become greater than unity in certain regions.

– The single spin asymmetry (SSA), measured in the scattering of a longitudinally polarized probe on an unpolarized target, is defined by

$$\text{SSA} = \frac{\int_0^{\pi} d\phi \Delta\sigma^{DVCS+BH} - \int_{\pi}^{2\pi} d\phi \Delta\sigma^{DVCS+BH}}{\int_0^{2\pi} d\phi (d\sigma^{DVCS+BH,\uparrow} + d\sigma^{DVCS+BH,\downarrow})}, \tag{38}$$

where $\Delta\sigma = d\sigma^{\uparrow} - d\sigma^{\downarrow}$ and $\uparrow$ and $\downarrow$ signify that the lepton is polarized along or against its direction of motion, respectively.

– The charge asymmetry (CA) in the scattering of an unpolarized probe on an unpolarized target:

$$\text{CA} = \Big\{\Big(\int_{-\pi/2}^{\pi/2} d\phi \Delta d^C\sigma^{DVCS+BH} - \int_{\pi/2}^{3\pi/2} d\phi \Delta d^C\sigma^{DVCS+BH}\Big)\Big/ \Big(\int_0^{2\pi} d\phi (d^+\sigma^{DVCS+BH} + d^-\sigma^{DVCS+BH})\Big)\Big\}, \tag{39}$$

where $\Delta d^C\sigma = d^+\sigma - d^-\sigma$ corresponds to the difference of the scattering with a positron probe and an electron probe.

In the small-x limit, required for the dipole approximation, and at large Q^2, AAA and CA are directly proportional to the real part of the DVCS amplitude, and SSA to the imaginary part of the unpolarised amplitude (cf. (30,40,43) of [27])[7].

[7] At large x one also gets a contribution from the polarised and helicity-flip DVCS amplitudes, $\tilde{\mathcal{H}}_1, \mathcal{E}_1, \tilde{\mathcal{E}}_1$, which are negligible in the small x region (cf. (24, 30) of [27])

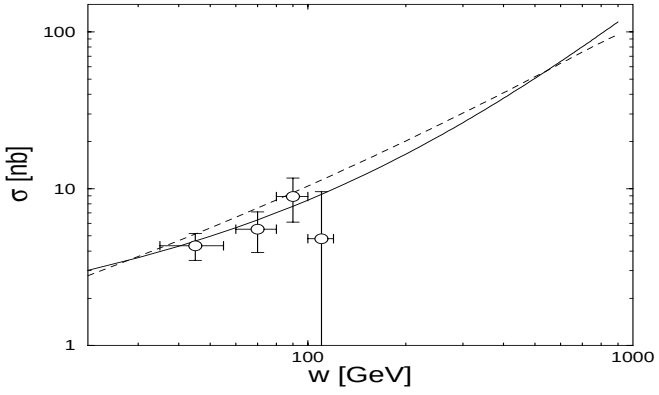

Fig. 14. The energy dependence of the photon level DVCS cross section at fixed $Q^2 = 4.5$ GeV^2: FKS (solid line); MFGS (dashed line)

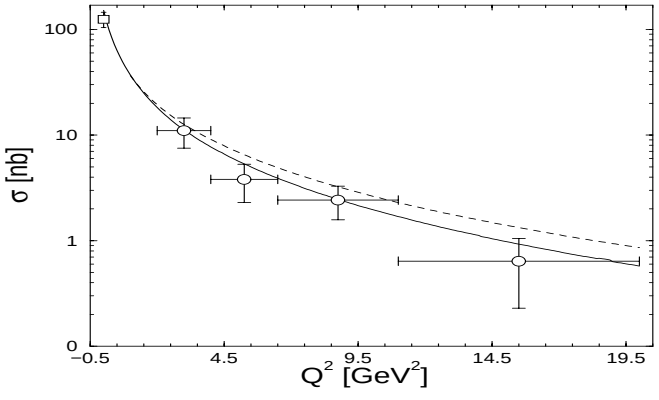

Fig. 15. The Q^2-dependence of the photon level DVCS cross section at fixed $W = 75$ GeV: FKS (solid line); MFGS (dashed line)

5 Results and conclusions

The Q^2 and W dependencies of the DVCS total cross-section of (30), obtained from our two dipole models, are compared with the H1 data [2] in Figs. 14, 15. In these figures, the vertical errors include statistical and systematic errors added in quadrature, and the horizontal errors indicate the bin width of the data. In making this comparison we have used the same value for the slope parameter, $B = 7$ GeV^{-2}, as that used by H1 to take into account the resolution and acceptance of their detector. It should be emphasized that the uncertainty in B implies an associated uncertainty in the normalization of the predictions, which could well be weakly Q^2 dependent. In addition, Donnachie and Dosch [11] have stressed that the real photon limit provides an important constraint, since the forward imaginary part can be inferred from fits to real photoabsorption data using the optical theorem, and their resulting value for the real photon cross section $\sigma(\gamma p \to \gamma p)$ is also shown in Fig. 15[8]. As can be seen, the consistency between the predictions and experiment is very encouraging for the basic features of the dipole models, despite the large statistical errors and the uncertainty in the slope parameter. Conversely, the close agreement between the predictions of the models out to energies well beyond the HERA region, despite the fact that one implements saturation effects approximately and one does not, means that the total cross-section is not a good discriminator between them. This is not unexpected, since DVCS

[8] We have actually increased their estimate by 4 % to allow for the value of β found in the FKS model. This change is much smaller than the estimated error

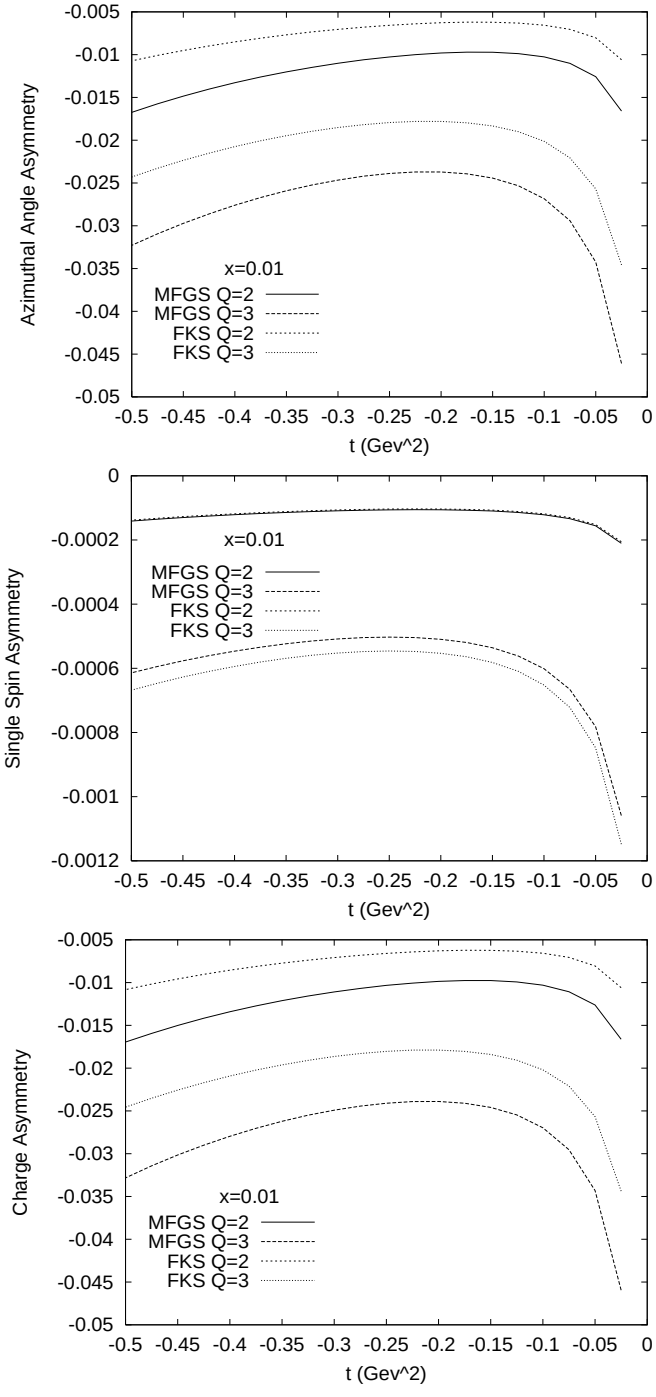

Fig. 16. Compendium of results on asymmetries for fixed $x = 10^{-2}$, at two values of $Q = 2, 3$ GeV, accessible in the HERA kinematic range

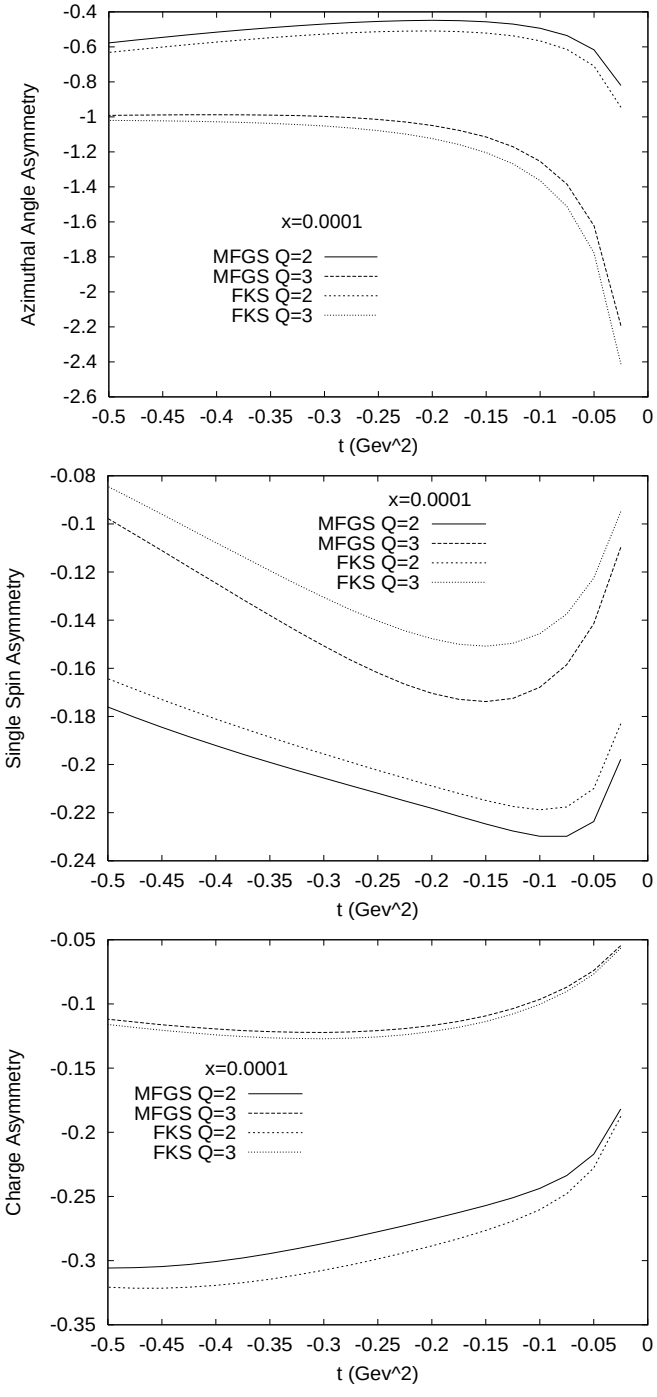

Fig. 17. Compendium of results on asymmetries for fixed $x = 10^{-4}$, at two values of $Q = 2, 3$ GeV, accessible in the HERA kinematic range. The results for SSA and AAA may be compared to Fig. 1 of [24] and for CA to Fig. 4a of [27]

is clearly a "softer" process than DIS, due to the presence of a real photon.

In Figs. 16, 17 we show results for the predicted asymmetries of (37, 38, 39) resulting from both models to indicate the overall size and spread of predictions expected in the small-x region ($x \in [10^{-2}, 10^{-4}]$) of HERA kinematics. The AAA and SSA results are for a positron and we use HERA kinematics with proton energy $E_p = 920$ GeV (i.e. $S = 4E_eE_p \approx 99,000$ GeV^2) to compute the value of $y = (W^2 + Q^2)/S$.

In conclusion, we observe that both models provide a good description of the available DVCS cross section data, without further tuning. We give predictions for the cross section at higher energies. A measurement of the asymmetries would allow the predicted phase of DVCS amplitude for both models to be tested.

Acknowledgements. We are happy to thank A. Freund and M. Strikman for helpful discussions and suggestions. We also thank R. Stamen and V. Guzey for helpful comments on the text. The work was supported by PPARC grant number PPA/G/0/1998 and a University of Manchester Research Studentship. M. M. was also supported by PPARC.

References

1. P.R. Saull, for the ZEUS Collab., Prompt photon production and observation of deeply virtual Compton scattering, Proc. EPS 99 (Tampere, Finland, July 1999), hep-ex/0003030
2. C. Adloff et al., H1 Collab., Phys. Lett. B **517**, 47 (2001)
3. N.N. Nikolaev, B.G. Zakharov, Z. Phys. C **49**, 607 (1991); Z. Phys. C **53**, 331 (1992); A.H. Mueller, Nucl. Phys. B **415**, 373 (1994); A.H. Mueller, B. Patel, Nucl. Phys. B **425**, 471 (1994)
4. E. Gotsman, E. Levin, U. Maor, Phys. Lett. B **425**, 369 (1998); Eur. Phys.J. C **10**, 689 (1999); and references therein
5. K. Golec-Biernat, M. Wüsthoff, Phys. Rev. D **59**, 014017 (1999); D **60**, 114023 (1999)
6. J.R. Forshaw, G. Kerley, G. Shaw, Phys. Rev. D **60**, 074012 (1999)
7. J.R. Forshaw, G. Kerley, G. Shaw, Nucl. Phys. A **675**, 80c (2000)
8. J. Forshaw, G.R. Kerley, G. Shaw, Colour dipole and saturation, Proc. DIS2000, Liverpool, April 2000, (World Scientific, 2001, p108), eds. J.A. Gracey, T. Greenshaw, hep-ph/007257
9. M. McDermott et al., Eur. Phys. J. C **16**, 641 (2000)
10. L. Frankfurt, M. McDermott, M. Strikman, JHEP **0103**, 045 (2001)
11. A. Donnachie, H.G. Dosch, Phys. Lett. B **502**, 74 (2001)
12. M.F. McDermott, The dipole picture of small x physics (a summary of the Amirim meeting), DESY 00-126, hep-ph/0008260
13. J.C. Collins, A. Freund, Phys. Rev. D **59**, 074009 (1999)
14. D. Mueller et al., Fortschr. Phys. **42**, 101 (1994); A.V. Radyushkin, Phys. Lett. B **380**, 417 (1996); X. Ji, Phys. Rev. Lett. **78**, 610 (1977); Phys. Rev. D **55**, 7114 (1997)
15. V.N. Gribov, L.N. Lipatov, Sov. J. Phys **15**, 438 (1972), 675; Yu.L. Dokshitzer, Sov. Phys. JETP **46**, 641 (1977); G. Altarelli., G. Parisi, Nucl Phys B **126**, 298 (1977)
16. A.V. Efremov, A.V. Radyushkin, Theor. Math. Phys. **42**, 97 (1980), Phys Lett. B **94**, 245 (1980); S.J. Brodsky, G.P. Lepage, Phys Lett. B **87**, 359 (1979); Phys. Rev. D **22**, 2157 (1980)

17. X. Ji et al., Phys. Rev. D **56**, 5511 (1997); A. Radyushkin, Phys. Rev. D **56**, 5554 (1997); I. Musatov, A. Radyushkin, Phys. Rev. D **61**, 074027 (2000)
18. A. Belitsky et al., Phys. Lett. B **474**, 163 (2000)
19. A. Belitsky et al., Phys. Lett. B **510**, 117 (2001)
20. N. Kivel, M.V. Polyakov, M. Vanderhaeghen, Phys. Rev. D **63**, 114014 (2001)
21. L. Frankfurt, A. Freund, M. Strikman, Phys. Rev. D **58**, 114001 (1998); *erratum* D **59**, 119901 (1999)
22. A. Donnachie, J. Gravelis, G. Shaw, Eur. Phys. J. C **18**, 539 (2001)
23. A. Freund, M. McDermott, Next-to-leading order evolution of generalized parton distributions for HERA and HERMES, hep-ph/0106115
24. A. Freund, M. McDermott, A next-to-leading order analysis of Deeply Virtual Compton Scattering, hep-ph/0106124
25. A. Freund, M. McDermott, A next-to-leading order QCD analysis of deeply virtual Compton scattering amplitudes, hep-ph/0106319
26. A. Radyushkin, Phys. Rev. D **59**, 014030 (1999)
27. A.Belitsky et al., Nucl. Phys. B **593**, 289 (2001)
28. H.G. Dosch et al., Phys. Rev. D **55**, 2602 (1997)
29. L. Frankfurt, V. Guzey, M. Strikman, Phys. Rev. D **58**, 094039 (1998)
30. H. Fraas, B.J. Read, D. Schildknecht, Nucl. Phys. B **86**, 346 (1975)
31. G. Shaw, Phys. Rev. D **47**, R3676 (1993); G. Shaw, Phys. Lett. B **228**, 125 (1989); P. Ditsas, G. Shaw, Nucl.Phys. B **113**, 246 (1976)
32. L. Frankfurt, A. Radyushkin, M. Strikman, Phys. Rev. D **55**, 98 (1997)
33. L. Frankfurt, W. Köpf, M. Strikman, Phys. Rev. D **54**, 3194 (1996); Phys. Rev. D **57**, 512 (1998)
34. H. Lai et al., CTEQ Collab. Phys. Rev. D **55**, 1280 (1997)
35. A. Freund, V. Guzey, Phys. Lett. B **462**, 178 (1999); Numerical methods in the LO evolution of non-diagonal parton distributions: the DGLAP case, hep-ph/9801388
36. M. Klein, THERA - electron proton scattering at $\sqrt{s} = 1$ TeV, Proc. DIS2000, Liverpool, April 2000, (World Scientific, 2001, p718), eds. J.A. Gracey, T. Greenshaw.